JGR Solid Earth

RESEARCH ARTICLE
10.1029/2020JB020923

Gravitationally Consistent Mean Barystatic Sea Level Rise From Leakage-Corrected Monthly GRACE Data

Henryk Dobslaw[1], Robert Dill[1], Meike Bagge[1], Volker Klemann[1], Eva Boergens[1], Maik Thomas[1,2], Christoph Dahle[1], and Frank Flechtner[1,3]

[1]Department 1: Geodesy, Deutsches GeoForschungsZentrum (GFZ), Potsdam, Germany, [2]Institute for Meteorology, Free University of Berlin, Berlin, Germany, [3]Chair of Physical Geodesy, Technical University of Berlin, Berlin, Germany

Abstract Gravitationally consistent solutions of the Sea Level Equation from leakage-corrected monthly-mean GFZ RL06 Gravity Recovery and Climate Experiment (GRACE) and GRACE Follow-On (GRACE-FO) Stokes coefficients reveal that barystatic sea level averaged over the whole global ocean was rising by 1.72 mm a^{-1} during the period April 2002 until August 2016. This rate refers to a truely global ocean averaging domain that includes all polar and semienclosed seas. The result corresponds to 2.02 mm a^{-1} mean barystatic sea level rise in the open ocean with a 1,000 km coastal buffer zone as obtained from a direct spatial integration of monthly GRACE data. The bias of +0.3 mm a^{-1} is caused by below-average barystatic sea level rise in close proximity to coastal mass losses induced by the smaller gravitational attraction of the remaining continental ice and water masses. Alternative spherical harmonics solutions from CSR, JPL, and TU Graz reveal open-ocean rates between 1.94 and 2.08 mm a^{-1}, thereby demonstrating that systematic differences among the processing centers are much reduced in the latest release. We introduce in this paper a new method to approximate spatial leakage from the differences of two differently filtered global gravity fields. A globally constant and time-invariant scale factor required to obtain full leakage from those filter differences is found to be 3.9 for GFZ RL06 when filtered with DDK3, and lies between 3.9 and 4.4 for other processing centers. Spatial leakage is estimated for every month in terms of global grids, thereby providing also valuable information of intrabasin leakage that is potentially relevant for hydrologic and hydrometeorological applications.

Plain Language Summary Satellite gravimetry as realized with the Gravity Recovery and Climate Experiment (GRACE) and GRACE Follow-On (GRACE-FO) missions is measuring tiny variations in the Earth's gravity field that are directly caused by divergent horizontal mass transports such as the melting of ice sheets and the corresponding discharge of melt water into the ocean basins. Between April 2002 and August 2016, this mass inflow caused sea level to rise by 1.72 mm each year as quantified from the latest GRACE reprocessing performed at our institute. The indirect observation principle of GRACE limits the spatial resolution so that highly localized mass loss signals are smeared out into the larger surrounding area, and possibly even from land into the ocean. We propose here a new method to quantify this so-called spatial leakage from the difference of gravity fields smoothed with slightly different spatial filters. A scale factor is obtained from exploiting the availability of two independent methods to estimate the mass component of sea level rise: The first method spatially integrates over the global gravity fields in all regions away from the coasts, and the second method utilizes a (leakage-corrected) mass distribution over the continents to calculate the gravitationally consistent distribution of water masses in all ocean basins. We estimate this scale factor as 3.9.

Key Points:
- Mean barystatic sea level rise is biased high by 0.3 mm a^{-1} when estimated with a 1,000 km coastal buffer zone
- Fractional spatial leakage in monthly GRACE gravity fields is quantified with two differently strong DDK filters
- Fractional leakage is scaled by a factor of 3.9 to make results from the Sea Level Equation consistent with open-ocean integrations

Correspondence to:
H. Dobslaw,
dobslaw@gfz-potsdam.de

Citation:
Dobslaw, H., Dill, R., Bagge, M., Klemann, V., Boergens, E., Thomas, M., et al. (2020). Gravitationally consistent mean barystatic sea level rise from leakage-corrected monthly GRACE data. *Journal of Geophysical Research: Solid Earth*, *125*, e2020JB020923. https://doi.org/10.1029/2020JB020923

Received 13 FEB 2020
Accepted 1 NOV 2020
Accepted article online 4 NOV 2020

1. Introduction

Satellite gravimetry as realized with the Gravity Recovery and Climate Experiment (GRACE) (Tapley et al., 2004) and GRACE Follow-On (GRACE-FO) missions (Landerer et al., 2020) has been revolutionary to many areas of the physical geosciences by providing unique and highly accurate estimates of long-term changes in terrestrial water storage variations, groundwater loss, ice mass changes, barystatic sea level variability, and viscoelastic deformations of the solid Earth (Tapley et al., 2019). Both GRACE and GRACE-FO precisely track the distance between two twin satellites following each other in a polar orbit of initially 500 km altitude with a separation of approximately 220 km. By evaluating orbit perturbations experienced by

the satellites at slightly different times, spatial variations in the Earth's gravity field can be inferred. Repeated measurements over months and years reveal moreover temporal variations indicative of mass changes in the Earth's solid and fluid compartments.

The indirect observing principle of GRACE, the dampening of spatial detail in the Earth's gravitational field with altitude, and the limited amount of sensor data accumulated over typically just 30 days used for a particular gravity field inversion restrain the spatial resolution of the GRACE time series. Moreover, gravity field models typically contain correlated errors that show a strong directional dependency: Correlations are in particular strong along the individual orbit and less pronounced between neighboring tracks observed at another day. Errors are thus characterized by distinct striping patterns that are aligned to the ground tracks in north-south direction. In the spectral domain, errors are smallest at spherical harmonic degrees 10–20 and grow exponentially for higher degrees. It is thus custom to suppress small-scale noise via spatial averaging with two-dimensional isotropic (Wahr et al., 1998) or anisotropic (Kusche, 2007) filters acting on the sphere. Smoothing in the spatial domain, however, also diminishes spatial gradients in geophysical signals and thus induces systematic errors into GRACE-based mass estimates known as spatial leakage.

Since the launch of GRACE in the year 2002, various methods have been proposed to account for spatial leakage. Classically, those effects were mitigated by extending the averaging region beyond the perimeter of a certain area by means of a so-called effective basin function (Swenson & Wahr, 2002). Regional averages under explicit consideration of spatial leakage can be also inferred via tailored sensivity kernels (Horwath & Dietrich, 2009) that allow for the introduction of prior knowledge about leakage sources via condition equations. Spatial leakage might also be treated via forward modeling, where a certain spatial pattern of mass anomalies in a region is assumed to be known and only a very reduced number of time-variable scaling parameters are estimated in a way that the residuals between forward-modeled gravity anomalies and observations from satellite gravimetry become minimal (Chen et al., 2013; Sasgen et al., 2012). However, additional observations about the spatial extent of the mass loss are required to setup the forward model, which are not readily available for every mass change phenomena observable with GRACE.

Alternatively, spatial leakage can be accounted for by filtering monthly-mean mass anomalies from global geophysical models in a way that is closely aligned to the postprocessing applied to monthly-mean gravity fields. Differences of filtered and unfiltered fields are related either multiplicatively or additively to the leakage-contaminated GRACE estimate for a certain region (Klees et al., 2007). Such a multiplicative approach has been applied for many years to the routinely processed globally gridded estimates of terrestrial water storage distributed via JPL's TELLUS website, which has been a popular access gateway to GRACE data for nongeodetic users (Landerer & Swenson, 2012). In extension to this approach, Vishwakarma et al. (2017) suggested that spatial leakage might be corrected from a cascade of spatial filters applied to the GRACE fields, thereby omitting the need for the introduction of a—potentially biased—global hydrological model into the GRACE data analysis process. It is the independence from any auxilliary information that sets the idea of Vishwakarma et al. (2017) favorably apart from other previously published spatial leakage methods, and we intend to follow that direction also in our analysis.

In this paper, we will present a new method to utilize differences between weaker and stronger smoothed monthly gravity fields from GRACE as a proxy for spatial leakage. To quantify its full amount, we will make use of the fact that the spatial distribution of excess water in the oceans causing barystatic sea level rise is accurately described by the Sea Level Equation (SLE) as utilized earlier in the context of satellite gravimetry by Hsu and Velicogna (2017) and Adhikari et al. (2019). A spatial integration of barystatic sea level over a large fraction of the ocean surface as seen by GRACE (direct approach) need to coincide with the numerical solution of the SLE averaged over the same region (SLE approach). The SLE solution itself solely relies on a—GRACE-based and leakage-corrected—mass distribution over the continents, thereby providing a way to constrain the total amount of spatial leakage. At the end, a spatial integration over the entire solution field of the SLE will provide a truly global mean barystatic sea level anomaly for a certain month. An spatial intregration over a 1,000 km buffer zone from the same solution field will provide an associated open-ocean barystatic sea level anomaly as it is typically derived from GRACE. The difference of the two results represents the estimation bias induced from omitting near-coastal regions in the integration that are experiencing below-average barystatic sea level rise due to the reduced gravitational attraction of the waning coastal ice masses.

The article is structured as follows: We present in section 2 how direct estimates of barystatic sea level from GRACE depend on various processing choices regarding low-degree spherical harmonics and a model for the present-day effects of glacial isostatic adjustment (GIA). Next, we introduce the SLE and demonstrate how coastal buffer zones of varying width bias the estimates of the global mean (section 3). We then describe a new method to quantify spatial leakage from scaled DDK filter pairs (section 4) and verify the approach by means of simulated GRACE gravity fields from a 5 years long end-to-end satellite mission simulation (section 5). The spatial leakage approximation is used to align results from the SLE with estimates from the direct approach, which provides the scale factor (section 6). Subsequently, we apply the leakage correction to calculate month-to-month variations in barystatic sea level (section 7), report trend estimates for different GRACE releases from other processing centers (section 8) and relate our results to previously published estimates of barystatic sea level rise (section 9). The paper closes with conclusions for the ongoing development of gridded Level-3 mass anomaly products from GRACE and GRACE-FO at GFZ (section 10).

2. Direct Spatial Integration of Barystatic Sea Level Rise

In line with Gregory et al. (2019), barystatic sea level rise is understood here as the mass component of the sea level rise, which is the change in hydrostatic pressure above the deformable ocean bottom. Barystatic sea level thus reflects the net transfer of water from continental storages as land-ice or groundwater into the oceans. It might be spatially variable due to the effects of gravitational attraction, Earth's rotation, and solid Earth deformation, and can be predicted from numerically solving the SLE (Farrell & Clark, 1976). Barystatic sea level rise can be also directly inferred from GRACE mass estimates over the oceans. Averaging over huge areas will diminish the contribution of residual ocean tides or circulation signals not accounted for by means of a priori information. Such background models are applied for both tidal and nontidal ocean mass variations during the processing of each gravity field from GRACE sensor data accumulated over one month. Regions in the vicinity of the coasts must not be included into the averaging region since those are expected to be subject of spatial leakage, which would bias the results. Buffer zones are often derived by smoothing a land mask with an isotropic Gaussian filter to exclude all regions with a notable continental influence (Johnson & Chambers, 2013). In the following, we will use five different buffer zones extending between 200 and 1,000 km off the coast.

We will focus specifically on the latest GFZ release 06 (RL06) of the monthly-mean gravity fields from GRACE and GRACE-FO (Dahle, Murböck, Flechtner, et al., 2019) with 179 individual solutions extending from April 2002 until November 2019. We start from standard Level-2 monthly-mean spherical harmonic coefficients publicly available online (isdcftp.gfz-potsdam.de), replace C_{21} and S_{21} with estimates from a normal equation combination of GRACE/GRACE-FO and satellite laser ranging (SLR) to several passive satellite targets processed at GFZ (abbreviated as GFZ-C in the following), replace C_{20} and C_{30} with results from SLR processed at Goddard Space Flight Center (Loomis & Rachlin, 2019) as given in GRACE Technical Note TN-14, augment geocenter motion estimates from values given in GRACE Technical Note TN-13 following Sun et al. (2016), subtract a model of present-day gravity rates induced by GIA (Peltier et al., 2018), and also subtract coseismic gravity changes associated with three megathrust earthquakes (Sumatra-Andaman 2004, Maule 2010, Tohoku-Oki 2011) with estimates published together with the global satellite-only gravity field model GOCO06s (Kvas, Mayer-Guerr, et al., 2019). Subsequently, all monthly fields are filtered with anisotropic DDK filters (Kusche, 2007) with different widths ranging from DDK8 (weakest filtering) to DDK1 (strongest smoothing), and finally, inverted mass anomalies are synthesized on a 1° latitude-longitude grid. Typically, trends from monthly sampled series are calculated in this paper from the time period April 2002 to August 2016 by concurrently estimating offset, trend, and harmonics with periods of 365.25, 182.625, and 161 days. Results for other periods as provided in section 9 are referenced explicitly.

Global-mean barystatic sea level trends are calculated from the postprocessed GFZ RL06 fields for different DDK filters and various ocean buffer zones. For the full ocean domain—which includes semienclosed basins as Baltic and Black Seas but excludes all inland water bodies like the Caspian Sea—we obtain an average rate of 1.50 mm a^{-1} for unfiltered fields (Table 1). This estimate gradually reduces when applying stronger filtering caused by increased spatial leakage of continental mass loss signals into the averaging domain. For the series filtered with DDK1, a rate of only 1.00 mm a^{-1} is obtained. For a buffer zone of 200 km, however, results are substantially larger and range between 1.71 and 2.13 mm a^{-1}, whereas for even larger buffer zones those estimates converge further toward 2.02 mm a^{-1} independently of the chosen spatial filter. We

Table 1
Global-Mean Barystatic Sea Level Rise (mm a^{-1}) Over the Period April 2002 to August 2016 Obtained From Directly Integrating Spatially the Postprocessed GFZ RL06 Mass Anomalies Over the Oceans, Which Are Filtered With Numerous Different Versions of the DDK Anisotropic Filter and With Various Buffer Zones Ranging From 0 to 1,000 km Off the Coast

DDK	Buffer distance to coast					
filter	0 km	200 km	400 km	600 km	800 km	1,000 km
none	1.50	2.00	1.96	1.98	1.83	2.03
DDK8	1.43	2.13	2.02	2.00	1.98	2.03
DDK7	1.41	2.13	2.02	2.00	1.99	2.03
DDK6	1.36	2.13	2.03	1.99	2.00	2.04
DDK5	1.33	2.11	2.04	2.00	2.00	2.05
DDK4	1.26	2.05	2.06	2.01	2.01	2.04
DDK3	1.22	2.01	2.07	2.03	2.00	2.02
DDK2	1.12	1.89	2.05	2.07	2.03	2.02
DDK1	1.00	1.71	1.92	2.05	2.09	2.11

thus interpret this value as a robust estimate for the barystatic mean sea level rise from GFZ RL06 over the open-ocean domain away from the continents.

We judge the GRACE postprocessing choices described above as optimal for GFZ RL06. It is, however, important to keep in mind that the treatment of the low-degree coefficients is critically important to derive global mean barystatic sea level estimates. We note that disregarding the C_{30} values from SLR as given in TN-14 from the year 2012 onward and using the native GRACE estimates instead does not alter the results (Table 2). Replacing C_{20} and C_{30} with the values obtained from a combination of SLR and GRACE at normal equation level that also delivers C_{21} and S_{21} (Dahle & Murböck, 2019; labeled as GFZ-C) led to slightly reduced rates (-0.04 mm a^{-1}) in the open ocean. Using C_{20} from SLR as processed by the Center for Space Research (Cheng & Ries, 2019) and published as TN-11 reduces the trends in the open ocean even further (-0.08 mm a^{-1}). Very similar results are also obtained with a SLR-only solution processed at GFZ by Koenig

Table 2
Apparent Mean Barystatic Sea Level Rise (mm a^{-1}) Over the Period April 2002 to August 2016 Obtained From Spatially Integrating Mass Anomalies Over the Oceans From GFZ RL06 DDK3 With Numerous Different Choices for the Low-Degree Harmonics and for Various Buffer Zones Ranging From 0 to 1,000 km Off the Coast

					Buffer distance to coast					
C_{30}	C_{20}	C_{21}	S_{21}	Deg. 1	0 km	200 km	400 km	600 km	800 km	1,000 km
TN-14[a]	TN-14	GFZ-C[b]	GFZ-C	TN-13[c]	1.22	2.01	2.07	2.03	2.00	2.02
GSM	TN-14	GFZ-C	GFZ-C	TN-13	1.23	2.02	2.07	2.04	2.01	2.03
GFZ-C	TN-14	GFZ-C	GFZ-C	TN-13	1.23	2.03	2.08	2.04	2.01	2.03
GFZ-C	GFZ-C	GFZ-C	GFZ-C	TN-13	1.21	2.00	2.05	2.00	1.97	1.98
GFZ-C	GFZ[d]	GFZ-C	GFZ-C	TN-13	1.20	1.97	2.02	1.96	1.92	1.93
GFZ-C	TN-11[e]	GFZ-C	GFZ-C	TN-13	1.20	1.97	2.02	1.97	1.93	1.94
GFZ-C	GSM[f]	GFZ-C	GFZ-C	TN-13	1.24	2.03	2.09	2.05	2.03	2.05
GSM	GSM	GFZ-C	GFZ-C	TN-13	1.23	2.03	2.08	2.05	2.02	2.04
GSM	GSM	GSM	GFZ-C	TN-13	1.22	2.01	2.06	2.02	2.00	2.02
GSM	GSM	GSM	GSM	TN-13	1.19	1.98	2.04	2.00	1.98	2.00
GSM	GSM	GSM	GSM	BW14[g]	1.02	1.73	1.75	1.67	1.61	1.61
GSM	GSM	GSM	GSM	GSM[h]	0.83	1.46	1.44	1.32	1.23	1.19

[a]C_{20} and C_{30} from SLR processed at Goddard Space Flight Center and published as TN-14. [b]C_{20}, C_{21}, S_{21}, and C_{30} from a combination of SLR and GRACE normal equations processed at GFZ (Dahle & Murböck 2019). [c]Degree-1 terms (C10, C11, and S11) following Sun et al. (2016) and published as TN-13. [d]C_{20} from SLR processed at GFZ (Koenig et al., 2019). [e]C_{20} from SLR processed at Center for Space Research (University of Texas) and published as TN-11. [f]Obtained from GRACE only and provided within the GSM monthly solution file. [g]Degree-1 terms (C10, C11, and S11) following Bergmann-Wolf et al. (2014). [h]Degree-1 terms (C10, C11, and S11) from GRACE are 0 by definition.

Table 3
Apparent Mean Barystatic Sea Level Rise (mm a^{-1}) Over the Period April 2002 to August 2016 Obtained From Spatially Integrating Mass Anomalies Over the Oceans From GFZ RL06 Filtered With DDK3 and C_{20} From TN-14 With Numerous Models of Glacial Isostatic Adjustment and With Various Buffer Zones Ranging From 0 to 1,000 km Off the Coast

	Buffer distance to coast					
GIA model	0 km	200 km	400 km	600 km	800 km	1,000 km
Peltier et al. (2018)	1.22	2.01	2.07	2.03	2.00	2.02
Geruo et al. (2013)	1.32	2.12	2.16	2.11	2.08	2.09
Steffen et al. (2017)	1.05	1.90	2.00	1.97	1.95	1.98
Sasgen et al. (2017)	1.08	1.89	1.99	1.97	1.98	2.03
Klemann et al. (2008)	1.06	1.80	1.86	1.83	1.83	1.87
VILMA: ICE-5G (VM2)	1.23	2.05	2.16	2.14	2.14	2.17
VILMA: ICE-6G (VM5a)	1.24	2.10	2.17	2.14	2.11	2.13
VILMA: ICE-6G (VM5a) + rot	1.16	2.00	2.08	2.04	2.03	2.06

et al. (2019), which results in a rate that is 0.09 mm a^{-1} lower than the value of 2.02 mm a^{-1} derived with the optimal processing. It is interesting to note that trends obtained with TN-14 are almost fully corroborated when using C_{20} and C_{30} from GRACE directly (+0.02 mm a^{-1}), which we take as additional evidence to prefer TN-14 over competing SLR estimates. Please note that it is still advantageous to utilize TN-14 instead of the native low-degree coefficients due to the smaller month-to-month variability in the values from TN-14. As a side note, we also present apparent trends in barystatic sea level when Degree-1 coefficients are either approximated from the method by Bergmann-Wolf et al. (2014), or are even entirely omitted. The substantial changes in the estimated sea level rates of about −0.41 and −0.83 mm a^{-1}, respectively, indicate that all low-degree coefficients must be augmented very carefully in the GRACE solution to obtain reliable trend estimates of this large-scale ocean signal.

We further recall that gravity changes caused by GIA in the upper mantle need to be reduced from the GRACE data before interpreting the residuals as long-term changes in barystatic sea level. The history of ice accumulation and melting on Earth during the last glacial cycle of approximately 120,000 years is a topic of ongoing research, and much progress has been made since the launch of GRACE both in terms of understanding the involved dynamics and modeling the present-day consequences (Whitehouse, 2018). Uncertainties in GIA forward models particularly arise from imprecise knowledge about the land ice history and the rheology of the Earth. For example, Li et al. (2018) combined global relative sea level data, crustal uplift rates obtained from coordinate series of Global Navigational Satellite Systems (GNSS) receivers, and peak gravity rates from satellite gravimetry with the aim to find best fitting 3-D mantle viscosity models in Fennoscandia and Laurentia. By considering both GRACE mass balance estimates and present-day uplift rates from GNSS, van der Wal et al. (2015) evaluated GIA models for Antarctica to identify regions of highest model uncertainties.

We therefore show apparent barystatic sea level trends when GIA is corrected by alternative model estimates frequently used for GRACE data analysis in the past (Table 3). Based on the ICE-5G glaciation history, the model by Geruo et al. (2013) leads to open-ocean barystatic sea level trends that are 0.07 mm a^{-1} larger than the rates obtained with the model by Peltier et al. (2018). A composite GIA model assembled by Steffen et al. (2017) for continental applications within the European Gravity Field Service for Emergency Management (Jäggi et al., 2019) leads to a somewhat reduced rate of 1.98 mm a^{-1}. Almost similar results as with the model by Peltier et al. (2018) are obtained for another empirical GIA model constrained by GNSS crustal uplift rates published by Sasgen et al. (2017).

We also note that exceptionally small barystatic sea level trends are obtained with present-day GIA-induced gravity rates calculated by Klemann et al. (2008) with the forward model VILMA (Martinec, 2000) as recently discussed in Uebbing et al. (2019). Those results are based on nowadays superseded assumptions about the Earth's viscosity structure. Recent computations with the same numerical code for ICE-5G (VM2) and ICE-6G (VM5a) lead to much higher open-ocean barystatic sea level trends (2.17 and 2.13 mm a^{-1}, respectively). It is interesting to note that considering the rotational potential perturbation in the formulation of the solid Earth deformation as proposed by Martinec and Hagedoorn (2014) reduces the misfit with

Table 4
Apparent Global-Mean Barystatic Sea Level Rise (mm a^{-1}) Over the Period April 2002 to August 2016 Obtained From Using the Land Mass Estimates From GFZ RL06 Filtered With Different Versions of the DDK Anisotropic Filter as Input to the Sea Level Equation (i.e., the SLE Method) With Various Buffer Zones Ranging From 0 to 1,000 km Off the Coast

	Buffer distance to coast						Bias
Filter	0 km	200 km	400 km	600 km	800 km	1,000 km	1,000 km
none	1.50	1.60	1.64	1.69	1.72	1.75	0.25
DDK8	1.43	1.53	1.57	1.61	1.65	1.68	0.23
DDK7	1.41	1.51	1.55	1.59	1.63	1.66	0.25
DDK6	1.36	1.45	1.49	1.53	1.57	1.59	0.23
DDK5	1.33	1.42	1.46	1.50	1.53	1.56	0.23
DDK4	1.26	1.35	1.38	1.42	1.45	1.47	0.21
DDK3	1.22	1.31	1.34	1.38	1.41	1.43	0.21
DDK2	1.12	1.20	1.24	1.27	1.30	1.32	0.21
DDK1	1.00	1.08	1.11	1.14	1.17	1.19	0.19

respect to the model by Peltier et al. (2018) to only +0.04 mm a^{-1}. The numerical results from Klemann et al. (2008) thus should not be included into any ensemble of equally probable estimates meant to characterize present-day uncertainties of contemporaneous GIA.

3. Global-Mean Ocean Mass From the SLE

We now use the monthly-mean mass distributions over the continents as input to the SLE as formulated by Tamisiea et al. (2010). Three iterations are performed with coast lines represented by spherical harmonics up to degree and order 180. The resulting spatially variable sea level patterns are subsequently integrated over the same buffered ocean masks used above for the direct approach. From Table 4, we note an important systematic increase in estimated mean barystatic sea level for larger buffer zones: Self-attraction causes a drop in relative sea level along coasts where strong continental mass losses occur. Ignoring those regions in the integration domain thus leads to an overestimation of the barystatic sea level rise. As a rule-of-thumb, we deduce that global mean barystatic sea level trends appear to be up to 0.3 mm a^{-1} higher when estimated from an ocean mask with a 1,000 km coastal buffer zone.

It is important to recall that all estimates above are obtained from the original Level-2 monthly gravity solutions of GRACE only (i.e., the so-called GSM fields), and no effort has been made to restore signal components removed during the dealiasing process of nontidal atmospheric and oceanic masses. We therefore report trends contained in RL05 (Dobslaw et al., 2013) and RL06 (Dobslaw et al., 2017) of the dealiasing model AOD1B for both SLE and the direct approach that are expressed in terms of equivalent barystatic sea level (Table 5). Specifically, we assess the monthly mean of the applied nontidal background model (i.e., the so-called GAC fields) that correspond to the monthly mean of the "glo" coefficients of AOD1B subtracted during the gravity field inversion (see Dahle, Murböck, Flechtner, et al., 2019). With the direct approach, we find insignificant trends ranging from −0.08 to −0.01 mm a^{-1} for GAC RL06, but values between −0.50

Table 5
Impact of Different Releases of the Nontidal Dealiasing Model AOD1B Subtracted During GRACE Gravity Field Processing on the Apparent Mean Barystatic Sea Level Rise in mm a^{-1} From Both the Direct Integration and the SLE Method With Various Buffer Zones Ranging From 0 to 1,000 km From the Coast

AOD1B	Estimation	Buffer distance to coast					
release	method	0 km	200 km	400 km	600 km	800 km	1,000 km
GAC RL05[a]	direct	−0.13	−0.41	−0.48	−0.50	−0.50	−0.50
GAC RL06[b]	direct	0.02	−0.08	−0.07	−0.05	−0.02	−0.01
GAC RL05[a]	SLE	0.02	0.02	0.02	0.02	0.02	0.02
GAC RL06[b]	SLE	0.02	0.02	0.02	0.02	0.02	0.02

[a]Applied in ITSG-Grace2016. [b]Applied in GFZ RL06, CSR RL06, JPL RL06, and ITSG-Grace2018.

to $-0.13\,\mathrm{mm\,a^{-1}}$ for RL05: This is related to a secular drift in the RL05 ocean model with regionally strong mass changes in the simulated dynamics (see, e.g., Figure 5 of Dobslaw et al., 2013). The application of AOD1B RL05 thus leads to higher values in apparent global mean barystatic sea level in the GSM fields that compensate for this drift in the background model. For all GRACE releases based on AOD1B RL05 it is thus required to restore the background model before estimating mass trends over the ocean domain. For RL06, this is obviously no longer necessary in view of the much larger errors induced by the necessary choices for a GIA model and the replacements for low-degree harmonics.

For completeness, we also use the atmospheric mass anomalies over the continents as given by AOD1B as input to the SLE. For RL06, we obtain apparent rates of $0.02\,\mathrm{mm\,a^{-1}}$ independently of the width of the buffer zone. The global atmospheric mass contained in AOD1B grows over time due to slowly rising temperatures and a corresponding higher water-holding capacity. The trend signal, however, is superimposed by interannual to decadal variations, rendering those small trends estimated for the selected averaging period as indeed plausible. We further note that results are basically identical for AOD1B RL05 and RL06 despite of the fact that atmospheric mass jumps related to occasional ECMWF model changes are present only in the older release (Fagiolini et al., 2015). We thus conclude that estimates of barystatic mean sea level from GRACE are no longer systematically biased by drifts or jumps when AOD1B RL06 is applied.

4. Spatial Leakage From DDK Pairs

As stated before, barystatic sea level can be calculated from monthly GRACE gravity fields in two fairly independent ways: First, a global mean estimate of barystatic sea level can be obtained from spatially integrating GRACE-based ocean bottom pressure anomalies over a certain spatial domain (i.e., the direct approach). This domain cannot be the whole ocean, since coastal regions are affected by spatial leakage, so that buffer zones extending several hundreds of kilometers off the continents are typically left out. Second, an observed mass distribution at the continents can be used to solve the SLE which provides a spatially variable mass-induced sea level anomaly available in all oceanic locations including the coastal seas (i.e., the SLE approach). Any solution of the SLE allows one to calculate regional averages over a certain spatial domain that can be readily compared with the results from the direct approach. The misfit between both methods is indicative of the bias in continental mass caused by spatial leakage across the coast.

Spatial leakage is introduced into GRACE gravity fields in various ways, since (i) sensors aboard the satellites are only tracing the (harmonically upward-continued) gravity field at orbit height, (ii) instrument data are sampled at discrete time steps and are partly smoothed in time to reduce the impact of sensor noise, (iii) only a finite number of gravity field parameters is solved for, and (iv) the application of spatially anisotropic postprocessing filters suppresses small-scale noise. Let $\Delta\sigma(\theta,\phi)$ be a surface mass distribution for a certain epoch obtained from Stokes coefficients ΔC_{lm}, ΔS_{lm} relative to a static gravity field as given by the GRACE Level-2 products (Wahr, 2009):

$$\Delta\sigma(\theta,\phi)=\frac{1}{3}a\rho_{\mathrm{ave}}\sum_{l=0}^{\infty}\sum_{m=0}^{l}\frac{2l+1}{1+k_l}\tilde{P}_{lm}(\cos\theta)(\Delta C_{lm}\cos(m\phi)+\Delta S_{lm}\sin(m\phi)), \tag{1}$$

with θ,ϕ being colatitude and eastward longitude, respectively, a is the radius of the Earth, $\rho_{\mathrm{ave}} = 5{,}517\,\mathrm{kg\,m^{-3}}$ is the average density of the Earth, k_l the Load Love Numbers, and $\tilde{P}_{lm}$ the normalized associated Legendre functions of degree l and order m.

Regional averages $\Delta\sigma_{\mathrm{reg}}$ can be obtained by spatially integrating over a certain area Ω on the spherical surface of the Earth

$$\Delta\sigma_{\mathrm{reg}}^{\mathrm{DDK3}}=\iint_{\Omega}\Delta\sigma^{\mathrm{DDK3}}(\theta,\phi)\,d\theta\,d\phi, \tag{2}$$

with $\Delta\sigma^{\mathrm{DDK3}}$ being obtained from postprocessed Level-2 Stokes coefficients filtered with the DDK3 filter. For a certain averaging region, the amount of full spatial leakage Λ^{DDK3} would be the difference between the true surface mass amount $\Delta\sigma$ and its approximation derived from DDK3-filtered Stokes coefficients ($\Delta\sigma^{\mathrm{DDK3}}$). As noted already by Klees et al. (2008), a change in signal at a certain location after applying different spatial averaging filters is indicative of the presence of spatial gradients in the mass distribution and thus spatial leakage. The so-called fractional spatial leakage λ for DDK3 is therefore obtained according to

$$\lambda_{\mathrm{reg}}^{\mathrm{DDK3}}=\Delta\sigma_{\mathrm{reg}}^{\mathrm{DDK4}}-\Delta\sigma_{\mathrm{reg}}^{\mathrm{DDK2}}. \tag{3}$$

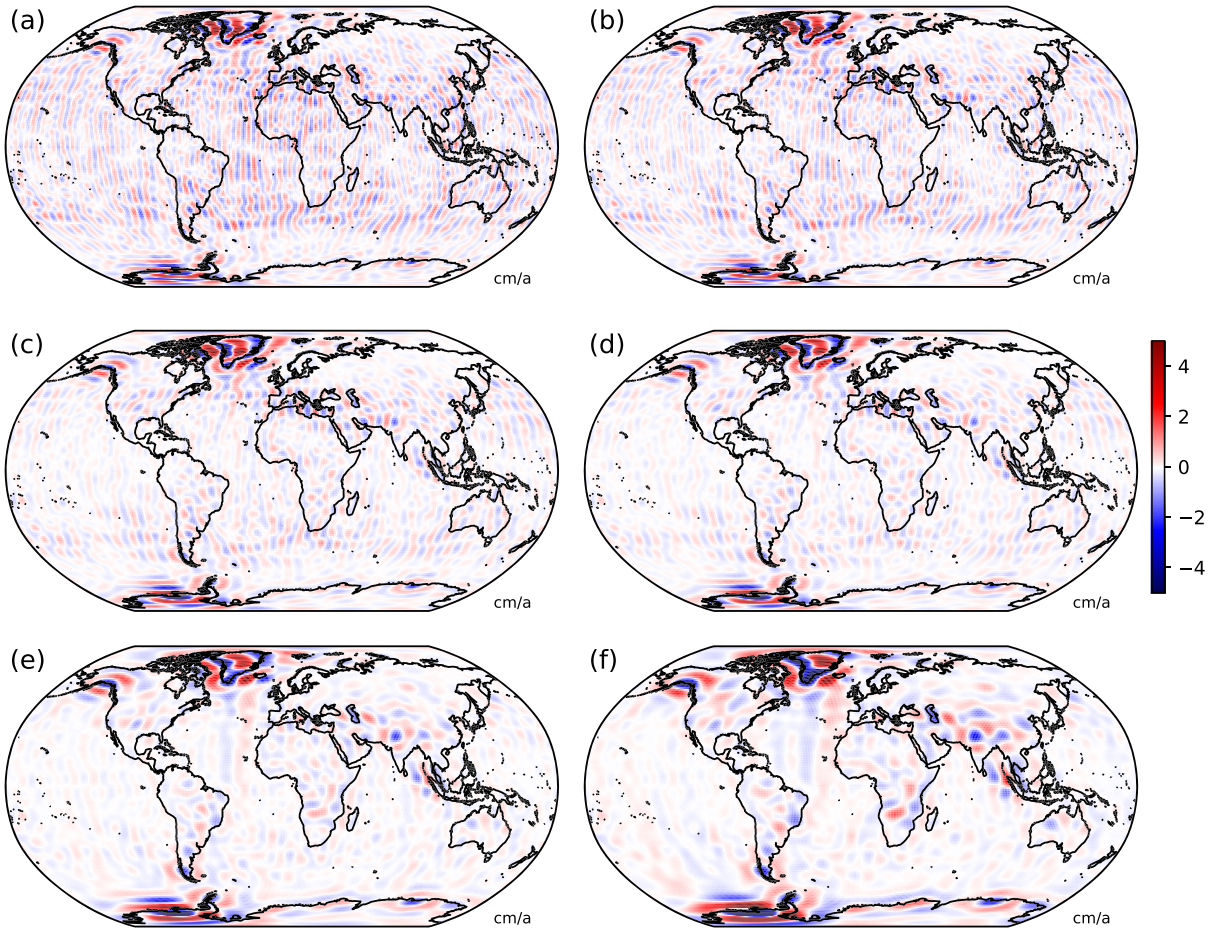

Figure 1. Maps of fractional leakage λ in trend estimates from GRACE GFZ RL06 for (a) λ^{DDK7} as obtained from $\Delta\sigma^{DDK8} - \Delta\sigma^{DDK6}$; (b) λ^{DDK6} as obtained from $\Delta\sigma^{DDK7} - \Delta\sigma^{DDK5}$; (c) λ^{DDK5} as obtained from $\Delta\sigma^{DDK6} - \Delta\sigma^{DDK4}$; (d) λ^{DDK4} as obtained from $\Delta\sigma^{DDK5} - \Delta\sigma^{DDK3}$; (e) λ^{DDK3} as obtained from $\Delta\sigma^{DDK4} - \Delta\sigma^{DDK2}$; and (f) λ^{DDK2} as obtained from $\Delta\sigma^{DDK3} - \Delta\sigma^{DDK1}$.

We are now going to compare various DDK filter pairs in order to identify regions affected most by spatial leakage, and to study similarities and differences found in the individual filter pairs in order to understand how much of the full spatial leakage Λ^{DDK} is contained in the fractional leakage estimate λ^{DDK} derived from a certain filter pair. Trends in equivalent water height are calculated from monthly sampled GFZ RL06 data for six different filter pairs (Figure 1). We note strong residual anisotropic noise for λ^{DDK7} (as derived from the difference of $\Delta\sigma^{DDK8}$ and $\Delta\sigma^{DDK6}$) that gradually reduces when moving toward λ^{DDK2}. Regions of strong coastal ice mass loss in Greenland, Alaska, Patagonia and Antarctica are nevertheless easily identified in any of the filter pairs, and also regions of groundwater loss as in the northwest of India are clearly apparent. We also note a checkerboard pattern at the position of the 2004 Sumatra-Andaman earthquake, possibly indicating postseismic gravity signals associated with that megathrust event not treated properly in the postprocessing of GRACE Level-2 gravity fields.

5. Method Verification With Simulated Gravity Fields

In order to corroborate our hypothesis that fractional leakage λ^{DDK} obtained from differences of DDK filter pairs indeed provide information about spatial leakage, we utilize a series of simulated gravity fields originally published by Flechtner et al. (2016). The data contains 60 individual monthly solutions covering the time span of 5 years and has been obtained from highly realistic end-to-end satellite mission performance simulations. Realistic orbits of both satellites as simulated from the synthetic time-variable gravity fields of the ESA Earth System Model (Dobslaw et al., 2015) represent key features of the GRACE mission, including altitude decay from 490 to 450 km, a varying satellite separation between 170 and 270 km, and temporary

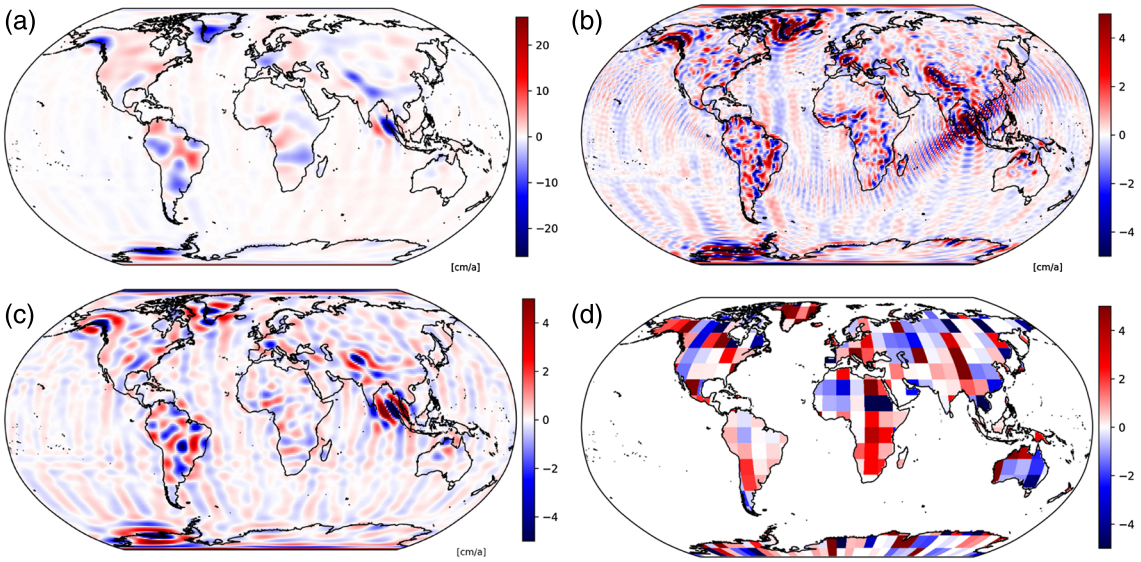

Figure 2. Testing the new method to estimate spatial leakage based on DDK filter pairs with 60 simulated GRACE-like monthly solutions of Flechtner et al. (2016) that cover a time period of 5 years: (a) surface mass ($\Delta\sigma^{DDK3}$) trend obtained from the DDK3-filtered monthly-mean global gravity fields, (b) true spatial leakage (Λ^{DDK3}) in the trend derived from the difference of DDK3 and the synthetic input gravity field from ESAESM (Dobslaw et al., 2015), (c) fractional leakage (λ^{DDK3}) in the trend derived from the difference of $\Delta\sigma^{DDK4}$ and $\Delta\sigma^{DDK2}$, and (d) linear regression of fractional leakage (λ^{DDK3}) against the full spatial leakage (Λ^{DDK3}) in the trend.

unfavorable repeat cycles as short as just 2 days. The simulations assume microwave ranging between the satellites with noise specifications taken from the GRACE instrument, while all other sensors rather correspond to the specifications of GRACE-FO. The final gravity field retrieval has been performed in line with the GFZ RL05 processing standards by applying the realistically perturbed dealiasing models of Dobslaw et al. (2016).

We use all 60 simulated gravity fields postprocessed with the DDK3 filter to estimate secular trends in surface mass $\Delta\sigma^{DDK3}$ (Figure 2). Prominent mass loss signals are clearly reflected in the retrievals which include ice sheet melting in Southern Greenland and West Antarctica, as well as mountain glacier mass loss in Alaska, the Himalayas, the Karakoram, and the European Alps. We also calculate spatial leakage Λ^{DDK3} from the difference of the synthetic input $\Delta\sigma$ and the retrieval $\Delta\sigma^{DDK3}$ (Figure 2b). The leakage map is dominated by Gibbs effects emanating from the Sumatra-Andaman earthquake, but we also find spatially coherent leakage signals in all regions of major mass loss. Please note that the color scale for Λ^{DDK3} differs by a factor of 5 from the plot of $\Delta\sigma^{DDK3}$.

We now calculate fractional leakage λ^{DDK3} for each of the 60 individual monthly solutions from the difference of the corresponding fields smoothed with DDK4 and DDK2 (Figure 2c). We find a considerable lack of detail in comparison with the true spatial leakage, which is plausible since the smallest scales of spatial leakage remain inaccessible even for a DDK4-filtered solution. However, all regions with strong spatial leakage are clearly identified also in λ^{DDK3}, whereas areas with small or almost no leakage effects (like the Sahara desert or Eastern Russia) are similarly quiet in the approximation.

For each 10° grid cell at the continents, we finally calculate linear regression coefficients between the secular trend estimates in fractional (λ^{DDK3}) and full leakage (Λ^{DDK3}). The obtained coefficients vary widely between −5 and 5, which is not surprising since many areas do not exhibit strong trend signals and are consequently also not affected by spatial leakage. In all regions with major ice mass loss in the synthetic input gravity fields, however, we find positive regression coefficients that reach values of 5 and more in the high-mountain regions of the Himalaya.

6. Scaling Coefficients for Full Spatial Leakage

In view of the various reasons for spatial leakage as listed above, it is obvious that $\Delta\sigma^{DDK4}_{reg}$ is already affected by spatial leakage itself so that the full leakage Λ^{DDK3}_{reg} must be somewhat higher than given by λ^{DDK3}_{reg}.

Table 6
Total Continental Mass Trends (Gt a^{-1}) for Differently Filtered Water Storage Anomalies and Associated Leakage Estimates From DDK Filter Pairs

	DDK7	DDK6	DDK5	DDK4	DDK3	DDK2
Filtered signal $\Delta\sigma_{\mathrm{Cnt}}^{\mathrm{DDK}}$ (Gt)	−530	−510	−499	−472	−459	−422
Fractional leakage $\lambda_{\mathrm{Cnt}}^{\mathrm{DDK}}$ (Gt)	−26.6	−30.8	−38.4	−40.6	−49.9	−82.8
Scale factor c^{DDK}	4.4	4.5	4.0	4.5	3.9	2.9
Full leakage $\Lambda_{\mathrm{Cnt}}^{\mathrm{DDK}}$ (Gt)	−117	−139	−154	−183	−195	−240
Leakage-restored signal $\Delta\sigma_{\mathrm{Cnt}}$ (Gt)	−647	−649	−653	−654	−654	−662
SLE 0 km (mm)	1.72	1.73	1.74	1.74	1.74	1.76
SLE 1,000 km (mm)	2.03	2.03	2.04	2.04	2.03	2.04
SLE bias 1,000 km (mm)	0.31	0.30	0.30	0.30	0.29	0.28

Note. Scale factors are estimated to match the barystatic sea level trends estimated from the direct integration over the oceans with 1,000 km buffer zone.

We therefore attempt to estimate a single time-invariant and globally applicable scaling coefficients c^{DDK3} to approximate full leakage from the differences of a certain DDK filter pair:

$$\Lambda_{\mathrm{reg}}^{\mathrm{DDK3}} = c^{\mathrm{DDK3}} \lambda_{\mathrm{reg}}^{\mathrm{DDK3}}. \tag{4}$$

To calculate this scaling coefficient, we make use of the unique opportunity in having available two complementary methods for infering barystatic sea level changes from GRACE (i.e., the direct and the SLE approach). We report mass trends integrated over all continental areas for different DDK filters together with the regionally averaged fractional leakage from the associated DDK filter pair (Table 6). The fractional leakage estimated from the associated DDK filter pairs, however, does not grow as strongly as the signal with increasing filter width, thereby indicating that some scaling is required to quantify the full leakage out of the fractional leakage obtained from the DDK pair.

A single time-invariant scaling coefficient is calculated by assuming that the total ocean mass increase amounts to approximately 650 Gt a^{-1}, which corresponds to a global mean barystatic sea level rise of 1.74 mm a^{-1} globally, and 2.02 mm a^{-1} for a 1,000 km buffer zone. This leads to scaling factors between 2.9 (DDK2) and 4.5 (DDK6). It would be plausible that those factors decrease with increasing filter strength, since the amount of leakage is increasingly dominated by the effect of the spatial filter over the other sources of leakage as stronger smoothing is applied. A strictly monotonic decay is, however, not found for GFZ RL06, and we therefore acknowledge substantial uncertainty in those scaling factors.

Subsequently, we evaluate the effect of the leakage approximation for various regions of the world that are known for severe mass loss during the GRACE period (Table 7). The mass estimates are always integrated over the extent of the region discretized on a 1° grid only, no attempt whatsoever is made to tweak the integration region. Spatial leakage is calculated from the associated DDK filter pair rescaled with the factor given in Table 6.

For all 10 regions selected, we note that the directly estimated signals monotonically decrease with stronger filtering, thereby indicating that more and more signal is leaking out of the region. For almost all filter pairs and averaging regions, the estimated full spatial leakage is negative, thereby increasing the directly estimated mass loss signal by a significant amount of, e.g. approximately 20% for Greenland or even up to 100% for the much smaller Baffin Island. We note very few exceptions of positive leakage for strong filtering with DDK2 in three regions with either small surface area extent (Iceland) or spatially highly scattered averaging regions (Baffin Island and the Canadian Arctic). We thus recommend to disregard leakage estimates for DDK2 since it involves filtering with the very strong DDK1 filter that smoothes signals over very large distances. Another exception is small positive leakage estimates (2 and 4 Gt a^{-1}) for the Alaskian Glaciers for DDK5 and DDK4, respectively, which is a rather narrow averaging region stretching along the coast of the Gulf of Alaska from east to west, and is thereby specifically prone to the influence of residual systematic errors in the GRACE mass estimates that are correlated in north-south direction.

We emphasize that the quantified spatial leakage is available in terms of global monthly grids that cover every place in the world. The information might be thus easily aggregated for arbitrary averaging regions

Table 7
Mass Trends ($Gt\,a^{-1}$) for Regions With Severe Mass Loss and Differently Filtered Mass Distributions From GFZ RL06 Together With Scaled Leakage Estimates From the Associated Rescaled DDK Filter Pairs

Region		DDK7	DDK6	DDK5	DDK4	DDK3	DDK2
Greenland	filtered signal $\Delta\sigma^{DDK}$	−182	−175	−172	−167	−165	−158
2,140e+3 km^2	full leakage Λ^{DDK}	−37	−41	−35	−35	−33	−59
	leakage restored $\Delta\sigma$	−219	−217	−207	−201	−197	−217
Ellesmere Island	filtered signal $\Delta\sigma^{DDK}$	−28	−27	−26	−25	−25	−22
310e+3 km^2	full leakage Λ^{DDK}	−5	−6	−7	−9	−12	−19
	leakage restored $\Delta\sigma$	−33	−33	−33	−34	−37	−41
Baffin Island	filtered signal $\Delta\sigma^{DDK}$	−27	−23	−22	−18	−16	−15
665e+3 km^2	full leakage Λ^{DDK}	−20	−22	−22	−24	−10	12
	leakage restored $\Delta\sigma$	−46	−46	−44	−42	−26	−4
Canadian Arctic	filtered signal $\Delta\sigma^{DDK}$	−4	−4	−3	−2	−2	−1
1,161e+3 km^2	full leakage Λ^{DDK}	−2	−3	−5	−7	−4	10
	leakage restored $\Delta\sigma$	−6	−7	−8	−9	−5	8
Alaska Glaciers	filtered signal $\Delta\sigma^{DDK}$	−35	−35	−35	−35	−36	−35
1,412e+3 km^2	full leakage Λ^{DDK}	−4	−2	2	4	−2	−21
	leakage restored $\Delta\sigma$	−40	−37	−32	−32	−38	−55
Russian Arctic	filtered signal $\Delta\sigma^{DDK}$	−10	−10	−10	−9	−8	−7
4,095e+3 km^2	full leakage Λ^{DDK}	−2	−3	−5	−6	−5	−5
	leakage restored $\Delta\sigma$	−12	−12	−14	−15	−13	−12
Svalbard	filtered signal $\Delta\sigma^{DDK}$	−2	−2	−2	−1	−1	−1
41e+3 km^2	full leakage Λ^{DDK}	−2	−2	−3	−3	−1	−1
	leakage restored $\Delta\sigma$	−4	−4	−4	−4	−2	−2
Iceland	filtered signal $\Delta\sigma^{DDK}$	−4	−3	−3	−2	−1	−1
78e+3 km^2	full leakage Λ^{DDK}	−5	−6	−6	−7	−2	3
	leakage restored $\Delta\sigma$	−9	−9	−9	−9	−3	1
Patagonia	filtered signal $\Delta\sigma^{DDK}$	−13	−13	−13	−11	−11	−8
721e+3 km^2	full leakage Λ^{DDK}	−1	−3	−6	−8	−13	−16
	leakage restored $\Delta\sigma$	−14	−16	−18	−20	−23	−24
Antarctica	filtered signal $\Delta\sigma^{DDK}$	−48	−47	−47	−44	−43	−39
12,302e+3 km^2	full leakage Λ^{DDK}	−5	−7	−13	−18	−20	−51
	leakage restored $\Delta\sigma$	−54	−54	−60	−62	−63	−90

and could thus provide information about intrabasin spatial leakage for hydrologic or hydrometeorological applications that is by now largely inaccessible for nonexpert users of satellite gravimetry data products.

7. Leakage-Corrected Barystatic Sea Level

We recall that scaling factors to account for spatial leakage (c^{DDK}) have been calculated to match only the trend signals in barystatic sea level rise. We now apply those—time-invariant and globally constant—factors to the fractional leakage estimate from the DDK filter pairs at the level of monthly solutions and compare the resulting sea level curves obtained from the direct integration for a 1,000 km buffer zone with the corresponding solution from the SLE utilizing the rescaled spatial leakage (Figure 3). We note very good consistency for results from the differently filtered versions. An outlier is apparent in the SLE solution in February 2015, where GRACE has been in temporary repeat orbit of just 2 days. We also note a flattening of the sea level rise signal after 2016, coinciding with the loss of accelerometer data from one of the satellites. This drop in sea level is not confirmed by independent observations and is suspected to be an artifact of the chosen accelerometer transplant approach (Bandikova et al., 2019).

For the differences between SLE and the direct integration, we note month-to-month differences as large as 3 mm, but no distinct seasonality or interannual variation. We find in general larger discrepancies after

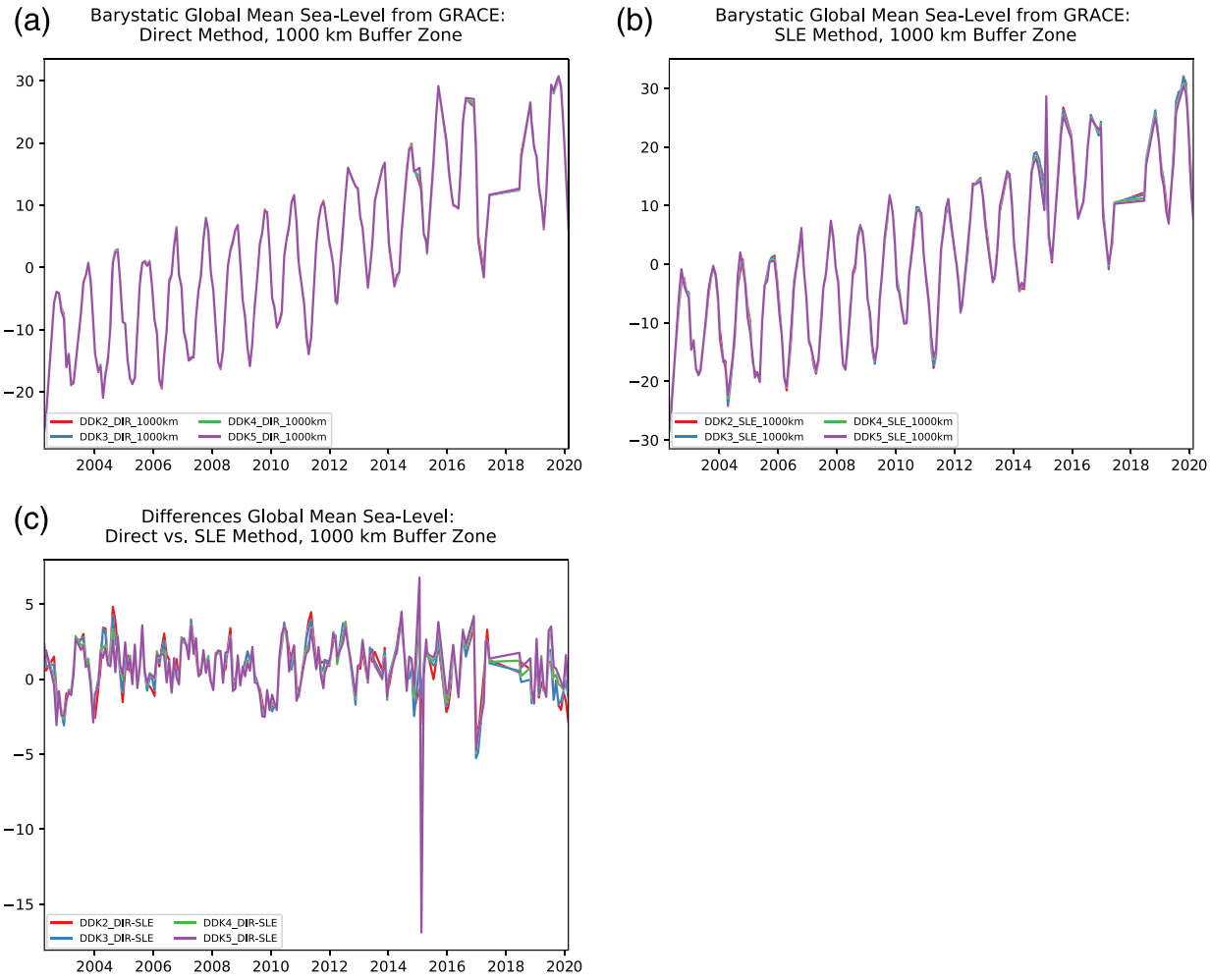

Figure 3. Apparent global mean barystatic sea level variations (mm) from monthly GFZ RL06 gravity models obtained from (a) direct integration with a 1,000 km buffer zone, (b) a solution of the Sea Level Equation (SLE) utilizing a continental leakage correction, and (c) the differences between direct and SLE method, each for different DDK filter versions.

Aug 2016, when accelerometer data on the GRACE-B spacecraft became unavailable. We also note a negative drift of the residuals after 2016 that continues well into the GRACE-FO mission period which is also affected by an underperforming accelerometer unit (again on the B satellite) and therefore also utilizes a transplant approach for the accelerometer data.

We also report the differences between the global mean barystatic sea level from the SLE solution for the unbuffered global ocean in comparison to the result for the 1,000 km buffer zone (Figure 4), revealing that the seasonal amplitude is increased by approximately 1 mm, and also the trend is overestimated by about 0.3 mm a^{-1} when only data away from the coasts is considered. This is expected, since barystatic sea level drops in the vicinity of near-coastal mass loss due to the reduced gravitational attraction of the remaining ice mass.

For one selected solution filtered with DDK3, we present globally gridded trend signals not corrected for continental leakage as used for the direct integration of barystatic sea level together with a SLE solution based on DDK3 corrected for spatial leakage from the scaled filter pair DDK4-DDK2 (Figure 5). We find clear differences in both solutions for most oceanic regions, namely negative anomalies in the southern part of the Indian Ocean and distinct positive anomalies in the southeastern and northwestern part of the Pacific. It remains open at this point if those signals represent large-scale changes in atmospheric wind that cause adjustments in the general ocean circulation not properly reflected in the nontidal ocean background model; consequences of ocean tide errors from partial tides with particularly long aliasing periods or rather

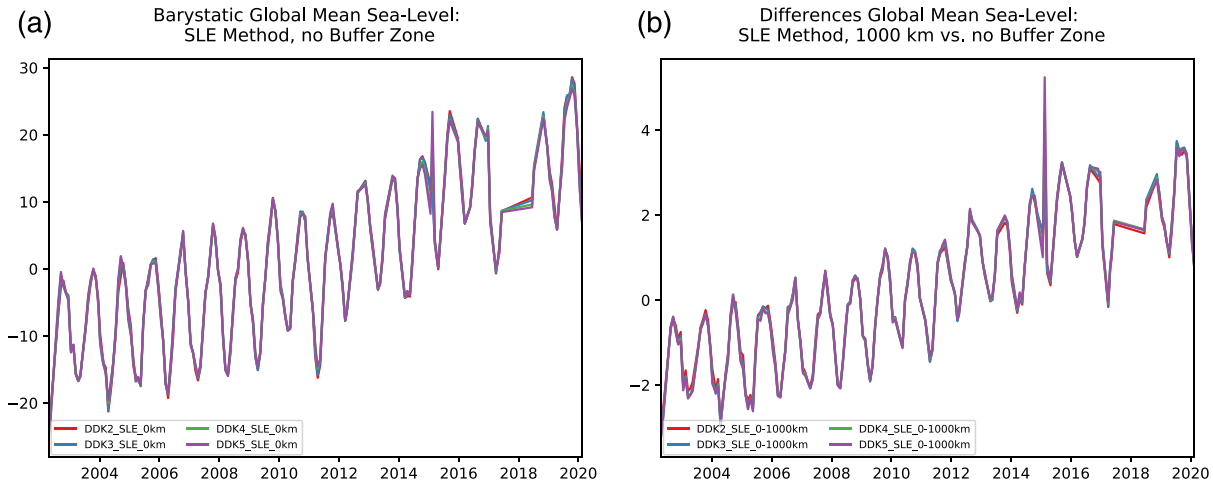

Figure 4. Global mean barystatic sea level variations (mm) from monthly GFZ RL06 gravity models obtained from the SLE method with continental leakage correction (a). Differences in global mean sea level from the same SLE solution arising from the application of a 1,000 km buffer zone (b).

artifacts of improper corrections of gravitational effects of viscoelastic redistribution of mass in the upper mantle and its associated feedbacks from sea level and Earth's rotation. We also note that regional trend patterns are discernable around Sumatra that are likely related to co- and postseismic signatures of the 2004 megathrust earthquake and somewhat weaker ruptures in more recent years in the immediate surroundings. In comparison to the directly estimated trends, we find the SLE solution to be much less spatially variable.

8. Trends in Other GRACE Releases

We now compare barystatic sea level trends obtained from four different alternative series of monthly-mean Stokes coefficients. We use CSR RL06 (Bettadpur, 2018) and JPL RL06 (Yuan, 2018) postprocessed in exactly the same way as the GFZ RL06 coefficients. We also include the most recent ITSG-Grace2018 solution from the Technical University of Graz (Kvas, Behzadpour, et al., 2019). For completeness, we also consider the nowadays outdated series ITSG-Grace2016 (Mayer-Gürr et al., 2016), which has been utilized in many sea level studies of the past. Please note that ITSG-Grace2016 applied the outdated version 05 of AOD1B (Dobslaw et al., 2013).

When C_{20} is consistently replaced with the monthly values given in TN-14, all four recent solutions lead to very close results for the direct approach with a 1,000 km ocean buffer zone. The estimates range from 1.94 (JPL RL06) to 2.08 mm a^{-1} (CSR), and thereby frame nicely the corresponding GFZ estimate (2.02 mm a^{-1}; Table 8). We note, however, that using the native C_{20} series delivered with ITSG-Grace2018 increases the estimated rate of barystatic sea level rise by more than 15% to 2.34 mm a^{-1}. This rate is substantially higher than results from all other tested series of C_{20} as reported before in Table 2. At this point, we cannot judge the relative accuracy of C_{20} from ITSG-Grace2018 with respect to TN-14 and leave this to future research. The

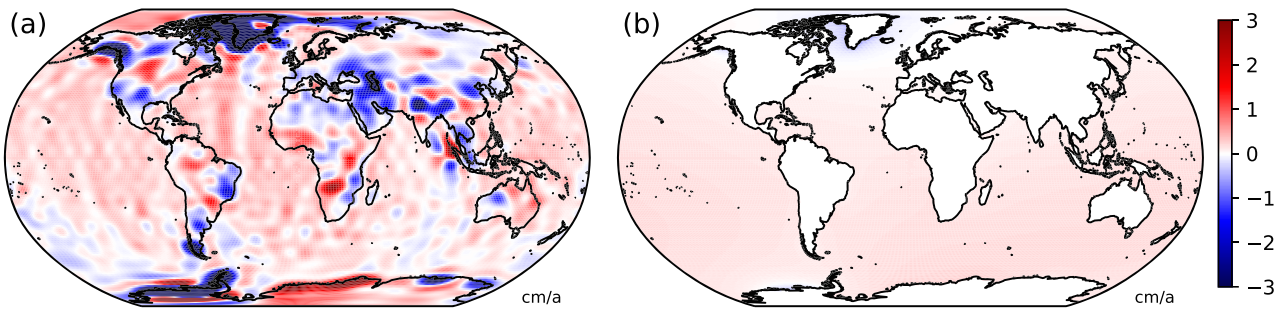

Figure 5. Spatially variable trends in barystatic sea level obtained directly from the GRACE gravity field time series GFZ RL06 (a) and obtained from the SLE method with continental leakage correction (b).

Table 8
Global Characteristics of Leakage-Corrected Sea Level Trends for Different Gravity Field Series Delivered as Level-2 Stokes Coefficients Filtered With DDK3, Whereas Spatial Leakage Is Estimated From the Differences Between DDK2 and DDK4

	GFZ RL06[a]	CSR RL06[a]	JPL RL06[a]	ITSG 2018[a,b]	ITSG 2018[b,c]	ITSG 2016[b,d]
Direct integr. 600 km (mm)	2.03	2.07	1.94	2.07	2.27	2.53
Direct integr. 800 km (mm)	2.00	2.05	1.92	2.05	2.29	2.54
Direct integr. 1,000 km (mm)	2.02	2.08	1.94	2.07	2.34	2.58
Filtered signal at continents $\Delta\sigma_{\mathrm{Cnt}}^{\mathrm{DDK3}}$ (Gt)	−459	−467	−424	−469	−504	−527
Fractional leakage $\lambda_{\mathrm{Cnt}}^{\mathrm{DDK3}}$ (Gt)	−49.9	−50.0	−46.3	−51.6	−51.6	−48.3
Scale factor c^{DDK3}	3.9	4.2	4.4	3.9	5.0	6.5
Full leakage $\Lambda_{\mathrm{Cnt}}^{\mathrm{DDK3}}$ (Gt)	−195	−210	−204	−204	−261	−316
Leakage-restored signal $\Delta\sigma_{\mathrm{Cnt}}$ (Gt)	−653	−678	−628	−673	−764	−843
SLE no buffer (mm)	1.74	1.81	1.67	1.79	2.04	2.24
SLE 600 km (mm)	1.94	2.01	1.87	2.00	2.26	2.49
SLE 800 km (mm)	1.98	2.05	1.91	2.04	2.31	2.54
SLE 1,000 km (mm)	2.02	2.08	1.94	2.07	2.34	2.58
Bias 1,000 km (mm)	0.28	0.27	0.27	0.28	0.30	0.33

[a]With C_{20} from TN-14. [b]With Degree-1 from TN-13 for CSR RL06. [c]With C_{20} from GSM. [d]With C_{20} from GSM and AOD1B RL05.

result nevertheless underlines the strong dependency of barystatic sea level estimates on precise measurements of C_{20} (and other low-degree coefficients) which certainly require the consideration of both GRACE sensor data and SLR multisatellite observations. An associated study about GFZ's efforts for a consistent combination of GRACE and SLR at the level of normal equations is currently being prepared.

Sea level rates obtained from the outdated series ITSG-Grace2016 with its native C_{20} estimate are even higher than for ITSG-Grace2018, but can be entirely explained by artificial drift in the applied background model AOD1B RL05 ($-0.5\ \mathrm{mm\ a^{-1}}$). Correcting properly for that effect leads to a sea level rate of $2.1\ \mathrm{mm\ a^{-1}}$, which is well in line with corresponding estimates from the most recent gravity field releases.

The strong impact of C_{20} is also reflected in pairwise differences of gridded mass trends for GFZ RL06 against the other GRACE releases considered in this paper (Figure 6). For the two solutions that include C_{20} from TN-14, we find only small differences that are mostly aligned in north-south oriented bands likely related to residual systematic errors in the series, as visible in, for example, the North Atlantic, or the eastern tropical Pacific. Gridded trend differences against ITSG-Grace2016 and ITSG-Grace2018 are instead dominated by the zonal pattern of C_{20} which particularly increases the trend signals at equatorial latitudes and therefore contributes to the much higher rates of global mean sea level rise obtained from those series.

For completeness, we also calculate fractional leakage from the DDK4-DDK2 filter pair for each of the other releases and estimate the associated scaling factors to align the direct estimate with the solution of the SLE. We find scaling factors between 3.9 (ITSG-Grace2018) and 4.4 (JPL RL06) that correspond quite nicely to the estimate for GFZ RL06 (3.9). We also note that scaling factors need to be considerably higher to account for the effects of native C_{20}, amounting to 5.0 (ITSG-Grace2018) or even 6.5 (ITSG-Grace2016). Albeit far from being a proof, we take those higher scaling factors as additional evidence to favor TN-14 over the native C_{20} processed by TU Graz.

9. Comparison to Published Sea Level Rates

We recall that all estimates of global mean barystatic sea level rise reported so far were calculated from data between GRACE launch and August 2016, which corresponds to the period 2002.4–2016.7. Global mean barystatic sea level is known to vary substantially on internannual to decadal timescales related to natural climate variability as discussed by, for example, Fasullo et al. (2013, 2018). We therefore relate a number of previously published results to the corresponding estimates obtained with GFZ RL06 (Table 9). Results are

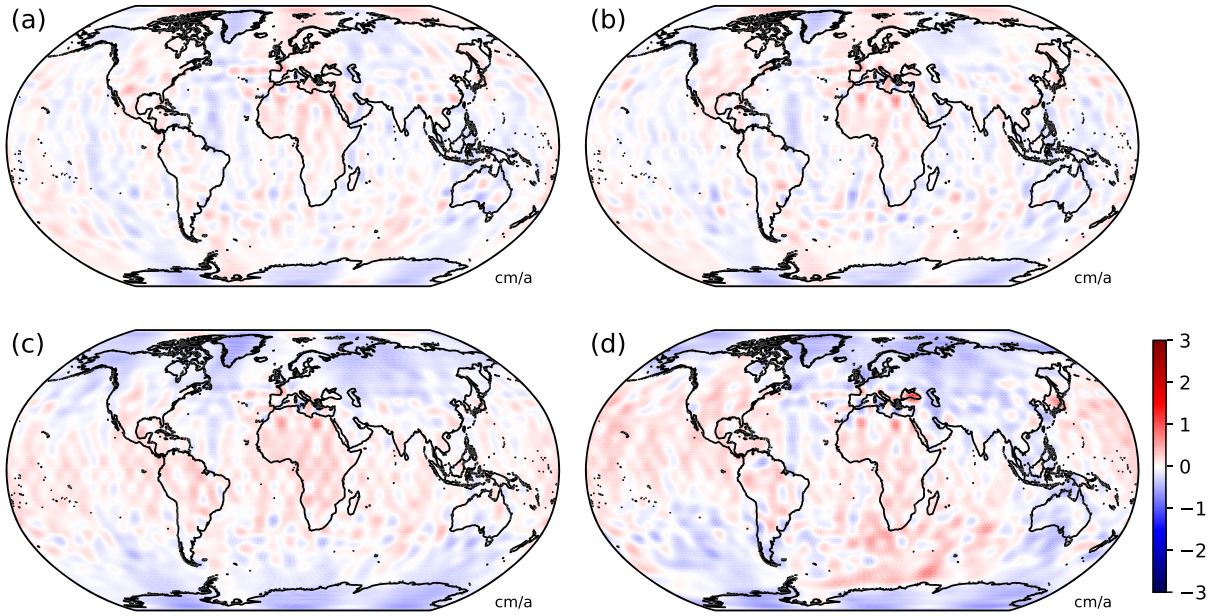

Figure 6. Differences in spatially variable trends in barystatic sea level obtained from different alternative series of monthly gravity fields with respect to GFZ RL06: CSR RL06 (a) and JPL RL06 (b) both processed with C_{20} from TN-14 as well as ITSG-Grace2018 (c) and ITSG-Grace2016 (d) processed with their native C_{20}. Note that ITSG-Grace2016 was processed with AOD1B RL05 and no effort was made to restore the nontidal ocean dealiasing product.

given both for the open ocean as obtained with a 1,000 km coastal buffer zone as well as for the global ocean from the spatial integration of the results of the SLE.

Dieng et al. (2015) uses 2.11 mm a^{-1} barystatic sea level rise in the open-ocean as obtained from the RL05 gravity field series of GFZ with the method of Johnson and Chambers (2013) to demonstrate the closure of the global sea level budget. Our estimated rates are 0.39 mm a^{-1} smaller for a 1,000 km buffer zone, and even 0.66 mm a^{-1} lower for the global ocean. The methodology of Johnson and Chambers (2013) has been recently evaluated in some detail by Uebbing et al. (2019), who in particular tediously examined the methodology to account for artifical drifts in AOD1B RL05 that largely became superfluous with the new release 06 of the background model. Based on the same gravity field series of GFZ RL05 as used by Dieng et al. (2015), Uebbing et al. (2019) obtain results that are 0.1 mm a^{-1} smaller than our estimate for the open ocean with a 1,000 km buffer zone, and 0.13 mm a^{-1} larger for the global ocean. More recently, Adhikari et al. (2019) calculated 1.79 mm a^{-1} from GFZ RL06 which is a little larger (+0.1 mm a^{-1}) than our estimate for the global ocean and would rather correspond to applying a ocean buffer zone of 200 km in our case. No effort was made in that study to account for the bias of omitting coastal areas exhibiting below-average sea level rise

Table 9
Barystatic Sea Level Trends From SLE Based on GFZ RL06 Filtered With DDK3, C_{20} From TN-14, and Leakage Correction in Comparison to Previously Published Estimates

				Published	Our result	
	Base period	Release	Method	estimate	No buffer	1,000 km
Dieng et al. (2015)[a]	2005.0–2014.0	GFZ RL05	direct	2.11	1.45	1.72
Uebbing et al. (2019)[a]	2002.6–2014.5	GFZ RL05	direct	1.43	1.30	1.53
Adhikari et al. (2019)	2005.0–2016.0	GFZ RL06	direct	1.79	1.69	1.97
Jeon et al. (2018)	2003.0–2015.0	CSR RL05	forward	2.14	1.35	1.58
Kim et al. (2019)[b]	2005.0–2016.0	CSR RL06	forward	2.07	1.69	1.97
Rietbroek et al. (2016)	2002.0–2015.0	GFZ RL05	inversion	1.08	1.32	1.56
Uebbing et al. (2019)[c]	2005.0–2013.9	GFZ RL05	inversion	1.68	1.45	1.72

[a]With the method of Johnson and Chambers (2013). [b]With the method of Jeon et al. (2018). [c]With the method of Rietbroek et al. (2016).

due to the reduced gravitational attraction of coastal mass loss, which we estimate to be −0.28 mm a^{-1} for the chosen time period.

By utilizing a forward modeling approach in combination with the RL05 gravity fields from CSR, Jeon et al. (2018) estimated 2.14 mm a^{-1} of global mean barystatic sea level rise, which is 0.56 mm a^{-1} higher than our open-ocean estimate, and even 0.79 mm a^{-1} higher than the our result for the global ocean. A more recent publication using the same methodology and the latest CSR RL06 gravity field series found 2.07 mm a^{-1} for a slightly different period, which is much closer to our open-ocean estimate of 1.97 mm a^{-1}, and almost halves the misfit for the global ocean average to just 0.48 mm a^{-1}.

Another alternative processing method to obtain global ocean mass rates is the joint inversion of satellite gravimetry data, GNSS elastic deformations, and (sometimes model-based) ocean bottom pressure as pioneered by Kusche and Schrama (2005) and Wu et al. (2006). For the GFZ RL05 gravity fields, Rietbroek et al. (2016) estimated a global barystatic sea level rise of 1.08 mm a^{-1} which is 0.24 mm a^{-1} lower than our estimate for the global ocean as obtained with the SLE. The methodology has been also used by Uebbing et al. (2019), who found with 1.68 mm a^{-1} a rate that is much more aligned to our estimate for the open ocean (1.72 mm a^{-1}). Since joint inversions are basically capable of providing estimates for the full unbuffered ocean, it would be prudent to reexamine the results of this study for specifically selected averaging regions, a topic that has unfortunately received very little attention in the paper by Uebbing et al. (2019).

10. Summary and Conclusions

Four new spherical harmonics solutions of global monthly gravity fields from GFZ, CSR, JPL, and TU Graz reveal mean barystatic sea level rates between 1.94 and 2.07 mm a^{-1} for the period April 2002 until August 2016 in the open ocean with a 1,000 km coastal buffer zone. The results are fully independent of the level of spatial smoothing applied. In contrast to releases of the past that often revealed important systematic differences between the centers, it is now possible to arbitrarily select any of the series to quantify global ocean mass changes. The SLE can be utilized to assess differences between open-ocean barystatic sea level directly observed by satellite gravimetry and a value representative for the whole ocean, which is biased by 0.3 mm a^{-1} due to below-average sea level rise in the direct vicinity of coastal mass loss induced by the reduced gravitational attraction acting on the water column.

Barystatic sea level rates are only similar across the processing groups when consistent estimates of the low-degree harmonics as in particular C_{20} are utilized. We recommend estimates given in TN-14, but note that more work is required to reveal reasons for the misfit with other C_{20} series as, for example, processed from GRACE as part of ITSG-Grace2018, which has the potential to change the estimated sea level rates by several tens of a millimeter per year. We further note that a model of GIA has been subtracted which is implicitly assumed to be error free. We judge the remaining errors in GIA to be smaller than the present-day uncertainties in C_{20} estimates but remind readers that GIA is a topic of ongoing research so that new findings might arise at any time.

The availability of two complementary methods to estimate barystatic sea level—the direct integration over a buffered ocean and the numerical solution of the SLE—allows to infer information about the magnitude of spatial leakage. We propose a new method to describe the spatial distribution of spatial leakage from the fractional leakage λ^{DDK} obtained from two differently filtered global gravity fields. A globally constant and time-invariant scale factor c^{DDK} is obtained by matching the results of the SLE—which requires as input solely a GRACE-based mass distribution at the continents that is corrected for the effects of spatial leakage—with the open-ocean barystatic sea level rise estimated directly from the gravity fields with an ocean buffer zone of 1,000 km. For GFZ RL06, this scale factor is found to be 3.9.

The scaled differences of differently filtered global gravity fields provide an estimate of spatial leakage in terms of a global grid. Since globally gridded mass estimates from portals as JPL's TELLUS or GFZ's GravIS website are important data sources for nongeodetic users, we will provide gridded monthly spatial leakage estimates as an additional data layer for both land and oceans from Release 06 Version 0002 of GravIS onward. The gridded spatial leakage estimate is thereby complementing the presently available data sets containing satellite-based mass anomalies and nontidal background models subtracted during the gravity field estimation process. We thereby give users the flexibility to explore mass variations for regions of interest with arbitrary shape. By publicly providing this additional leakage information, spatial averages from those

grids will converge further toward results obtained with specifically processed time series as available in the literature that usually account for the effects of spatial leakage by means of specifically tailored methods.

Over the oceans, the quantification of the spatially variable barystatic sea level variations by means of the SLE will allow to separate bottom pressure variations related to mass inflow from the continents from signals induced by the internal redistribution of water masses. The most important processes here are ocean tides and the general ocean circulation, which are meant to be removed from the gravity fields via known to be imperfect background models. We intend to use this information about the residual ocean circulation signals in the gravity fields for the development of the next generation of nontidal ocean background models.

Data Availability Statement

All GRACE and GRACE-FO data used in this study were submitted to GFZ's Information System and Data Center (ISDC), which is the official data repository for all German mission elements and ensures a version-controlled long-term availability of data products without any charges for users. Level-2 gravity fields (Dahle, Flechtner, et al., 2019) stored in ISDC are available via ftp://isdcftp.gfz-potsdam.de/grace/Level-2 website. Multisatellite SLR solutions (Dahle & Murböck, 2019) are provided via ftp://isdcftp.gfz-potsdam.de/grace/DOCUMENTS/TECHNICAL_NOTES/ website. Gridded Level-3 mass anomalies for ocean (Dobslaw et al., 2019) and land (Boergens et al., 2019) that also include the newly developed spatial leakage estimate are available from ftp://isdcftp.gfz-potsdam.de/grace/GravIS/ website. The data can be moreover interactively explored via a graphical interface available at https://gravis.gfz-potsdam.dewebsite.

Acknowledgments
We are very grateful to Jennifer Bonin and an anonymous reviewer for their insightful comments and helpful suggestions that allowed us to improve the article substantially. In addition, we would like to thank the editor Paul Tregoning for the attentive processing of our manuscript. This work has been supported by the German Research Foundation (Grant no. DO 1311/4-1) as part of the research group NEROGRAV (FOR 2736). Numerical simulations were performed at Deutsches Klimarechenzentrum (DKRZ). M. B. was funded by the PalMod project "German climate modeling initiative" (FKZ: 01LP1502E) supported by the German Federal Ministry of Education and Research (BMBF) as a Research for Sustainability initiative (FONA). V. K. contributed both to the PalMod project (FKZ: 01LP1503A) and the Helmholtz project "Advanced Earth system Modeling Capacity ESM." Funding for E. B. was available from the Horizon2020 project "Global Gravity-based Groundwater Product" of the European Union (Grant Agreement No. 870353). Open access funding enabled and organized by Projekt DEAL.

References

Geruo, A., Wahr, J., & Zhong, S. (2013). Computations of the viscoelastic response of a 3-D compressible Earth to surface loading: An application to Glacial Isostatic Adjustment in Antarctica and Canada. *Geophysical Journal International*, *192*(2), 557–572. https://doi.org/10.1093/gji/ggs030

Adhikari, S., Ivins, E. R., Frederikse, T., Landerer, F. W., & Caron, L. (2019). Sea-level fingerprints emergent from GRACE mission data. *Earth System Science Data*, *11*(2), 629–646. https://doi.org/10.5194/essd-11-629-2019

Bandikova, T., McCullough, C., Kruizinga, G. L., Save, H., & Christophe, B. (2019). GRACE accelerometer data transplant. *Advances in Space Research*, *64*(3), 623–644. https://doi.org/10.1016/j.asr.2019.05.021

Bergmann-Wolf, I., Zhang, L., & Dobslaw, H. (2014). Global eustatic sea-level variations for the approximation of geocenter motion from GRACE. *Journal of Geodetic Science*, *4*(1), 37–48. https://doi.org/10.2478/jogs-2014-0006

Bettadpur, S. V. (2018). UTCSR level-2 processing standards document for level-2 product release 0006. GRACE Publication 327-742.

Boergens, E., Dobslaw, H., & Dill, R. (2019). *GFZ GravIS RL06 continental water storage anomalies (level-3 product). V. 0002.* Potsdam, Germany: GFZ Data Services. https://doi.org/10.5880/GFZ.GRAVIS_06_L3_TWS

Chen, J. L., Wilson, C. R., & Tapley, B. D. (2013). Contribution of ice sheet and mountain glacier melt to recent sea level rise. *Nature Geoscience*, *6*(7), 549–552. https://doi.org/10.1038/ngeo1829

Cheng, M., & Ries, J. C. (2019). *Monthly estimates of C20 from 5 SLR satellites based on GRACE RL06 models.* Austin, TX: Center for Space Research, University of Texas.

Dahle, C., Flechtner, F., Murböck, M., Michalak, G., Abrykosov, O., Reinhold, A., & König, R. (2019). *GRACE geopotential GSM coefficients GFZ RL06*. Potsdam, Germany: GFZ Data Services. https://doi.org/10.5880/GFZ.GRACE_06_GSM

Dahle, C., & Murböck, M. (2019). *Post-processed GRACE/GRACE-FO geopotential GSM coefficients GFZ RL06 (level-2B product) V. 0002.* Potsdam, Germany: GFZ Data Services. https://doi.org/10.5880/GFZ.GRAVIS_06_L2B

Dahle, C., Murböck, M., Flechtner, F., Dobslaw, H., Michalak, G., Neumayer, K. H., & Förste, C. (2019). The GFZ GRACE RL06 monthly gravity field time series: Processing details and quality assessment. *Remote Sensing*, *11*(18), 2116. https://doi.org/10.3390/rs11182116

Dieng, H. B., Cazenave, A., Von Schuckmann, K., Ablain, M., & Meyssignac, B. (2015). Sea level budget over 2005-2013: Missing contributions and data errors. *Ocean Science*, *11*(5), 789–802. https://doi.org/10.5194/os-11-789-2015

Dobslaw, H., Bergmann-Wolf, I., Dill, R., Forootan, E., Klemann, V., Kusche, J. J., & Sasgen, I. (2015). The updated ESA Earth System Model for future gravity mission simulation studies. *Journal of Geodesy*, *89*(5), 505–513. https://doi.org/10.1007/s00190-014-0787-8

Dobslaw, H., Bergmann-Wolf, I., Dill, R., Poropat, L., Thomas, M., Dahle, C., & Flechtner, F. (2017). A new high-resolution model of non-tidal atmosphere and ocean mass variability for de-aliasing of satellite gravity observations: AOD1B RL06. *Geophysical Journal International*, *211*(1), 263–269. https://doi.org/10.1093/gji/ggx302

Dobslaw, H., Bergmann-Wolf, I., Forootan, E., Dahle, C., Mayer-Gürr, T., Kusche, J., & Flechtner, F. (2016). Modeling of present-day atmosphere and ocean non-tidal de-aliasing errors for future gravity mission simulations. *Journal of Geodesy*, *90*(5), 1–14. https://doi.org/10.1007/s00190-015-0884-3

Dobslaw, H., Boergens, E., & Dill, R. (2019). *GFZ GravIS RL06 ocean bottom pressure anomalies (level-3 product). V. 0002*. Potsdam, Germany: GFZ Data Services. https://doi.org/10.5880/GFZ.GRAVIS_06_L3_OBP

Dobslaw, H., Flechtner, F., Bergmann-Wolf, I., Dahle, C., Dill, R., Esselborn, S., & Thomas, M. (2013). Simulating high-frequency atmosphere-ocean mass variability for dealiasing of satellite gravity observations: AOD1B RL05. *Journal of Geophysical Research: Oceans*, *118*, 3704–3711. https://doi.org/10.1002/jgrc.20271

Fagiolini, E., Flechtner, F., Horwath, M., & Dobslaw, H. (2015). Correction of inconsistencies in ECMWF's operational analysis data during de-aliasing of GRACE gravity models. *Geophysical Journal International*, *202*(3), 2150–2158. https://doi.org/10.1093/gji/ggv276

Farrell, W. E., & Clark, J. a. (1976). On postglacial sea level. *Geophysical Journal of the Royal Astronomical Society*, *46*(3), 647–667. https://doi.org/10.1111/j.1365-246X.1976.tb01252.x

Fasullo, J. T., Boening, C., Landerer, F. W., & Nerem, R. S. (2013). Australia's unique influence on global sea level in 2010–2011. *Geophysical Research Letters*, *40*, 4368–4373. https://doi.org/10.1002/grl.50834

Flechtner, F., Neumayer, K. H. K. H., Dahle, C., Dobslaw, H., Fagiolini, E., Raimondo, J. C. J. C., & Güntner, A. (2016). What can be expected from the GRACE-FO laser ranging interferometer for Earth science applications? *Surveys in Geophysics*, *37*(2), 453–470. https://doi.org/10.1007/s10712-015-9338-y

Gregory, J. M., Griffies, S. M., Hughes, C. W., Lowe, J. A., Church, J. A., Fukimori, I., & van de Wal, R. S. W. (2019). Concepts and terminology for sea level: Mean, variability and change, both local and global. *Surveys in Geophysics*, *40*(6), 1251–1289. https://doi.org/10.1007/s10712-019-09525-z

Horwath, M., & Dietrich, R. (2009). Signal and error in mass change inferences from GRACE: The case of Antarctica. *Geophysical Journal International*, *177*(3), 849–864. https://doi.org/10.1111/j.1365-246X.2009.04139.x

Hsu, C. W., & Velicogna, I. (2017). Detection of sea level fingerprints derived from GRACE gravity data. *Geophysical Research Letters*, *44*, 8953–8961. https://doi.org/10.1002/2017GL074070

Jäggi, A., Weigelt, M., Flechtner, F., Güntner, A., Mayer-Gürr, T., Martinis, S., & Shabanloui, A. (2019). European Gravity Service for Improved Emergency Management (EGSIEM)—From concept to implementation. *Geophysical Journal International*, *218*(3), 1572–1590. https://doi.org/10.1093/gji/ggz238

Jeon, T., Seo, K. W., Youm, K., Chen, J., & Wilson, C. R. (2018). Global sea level change signatures observed by GRACE satellite gravimetry. *Scientific Reports*, *8*(1), 1–10. https://doi.org/10.1038/s41598-018-31972-8

Johnson, G. C., & Chambers, D. P. (2013). Ocean bottom pressure seasonal cycles and decadal trends from GRACE Release-05: Ocean circulation implications. *Journal of Geophysical Research: Oceans*, *118*, 4228–4240. https://doi.org/10.1002/jgrc.20307

Kim, J., Seo, K., Jeon, T., Chen, J., & Wilson, C. R. (2019). Missing hydrological contribution to sea level rise. *Geophysical Research Letters*, *46*, 12,049–12,055. https://doi.org/10.1029/2019GL085470

Klees, R., Revtova, E. A., Gunter, B. C., Ditmar, P., Oudman, E., Winsemius, H. C., & Savenije, H. H. (2008). The design of an optimal filter for monthly GRACE gravity models. *Geophysical Journal International*, *175*(2), 417–432. https://doi.org/10.1111/j.1365-246X.2008.03922.x

Klees, R., Zapreeva, E. A., Winsemius, H. C., & Savenije, H. H. (2007). The bias in GRACE estimates of continental water storage variations. *Hydrology and Earth System Sciences*, *11*(4), 1227–1241. https://doi.org/10.5194/hess-11-1227-2007

Klemann, V., Martinec, Z., & Ivins, E. R. (2008). Glacial isostasy and plate motion. *Journal of Geodynamics*, *46*(3–5), 95–103. https://doi.org/10.1016/j.jog.2008.04.005

Koenig, R., Schreiner, P., & Dahle, C. (2019). *Monthly estimates of C(2,0) generated by GFZ from SLR satellites based on GFZ GRACE/GRACE-FO RL06 background models*. Potsdam, Germany: GFZ Data Services. https://doi.org/10.5880/GFZ.GRAVIS_06_C20_SLR

Kusche, J. (2007). Approximate decorrelation and non-isotropic smoothing of time-variable GRACE-type gravity field models. *Journal of Geodesy*, *81*(11), 733–749. https://doi.org/10.1007/s00190-007-0143-3

Kusche, J., & Schrama, E. J. O. (2005). Surface mass redistribution inversion from global GPS deformation and Gravity Recovery and Climate Experiment (GRACE) gravity data. *Journal of Geophysical Research*, *110*, B09409. https://doi.org/10.1029/2004JB003556

Kvas, A., Behzadpour, S., Ellmer, M., Klinger, B., Strasser, S., Zehentner, N., & Mayer-Gürr, T. (2019). ITSG-Grace2018: Overview and evaluation of a new GRACE-only gravity field time series. *Journal of Geophysical Research: Solid Earth*, *124*, 9332–9344. https://doi.org/10.1029/2019JB017415

Kvas, A., Mayer-Guerr, T., Krauss, S., Brockmann, J. M., Schubert, T., Schuh, W. D., & Jaeggi, A. (2019). The satellite-only gravity field model GOCO06s. European Geophysical Union General Assembly.

Landerer, F. W., Flechtner, F., Save, H., Webb, F., Bandikova, T., Bertiger, W. I., & Yuan, D. N. (2020). New observations of global mass change: Extending the satellite data record with GRACE Follow-On. *Geophysical Research Letters 47*, e2020GL088306. https://doi.org/10.1029/2020GL088306

Landerer, F. W., & Swenson, S. C. (2012). Accuracy of scaled GRACE terrestrial water storage estimates. *Water Resources Research*, *48*, W04531. https://doi.org/10.1029/2011WR011453

Li, T., Wu, P., Steffen, H., & Wang, H. (2018). In search of laterally heterogeneous viscosity models of glacial isostatic adjustment with the ICE-6G_C global ice history model. *Geophysical Journal International*, *214*(2), 1191–1205. https://doi.org/10.1093/gji/ggy181

Loomis, B. D., & Rachlin, K. E. (2019). *NASA GSFC SLR C20 and C30 solutions*. Greenbelt, MD: Goddard Space Flight Center.

Martinec, Z. (2000). Spectral-finite element approach to three-dimensional viscoelastic relaxation in a spherical earth. *Geophysical Journal International*, *142*(1), 117–141. https://doi.org/10.1046/j.1365-246x.2000.00138.x

Martinec, Z., & Hagedoorn, J. (2014). The rotational feedback on linear-momentum balance in glacial isostatic adjustment. *Geophysical Journal International*, *199*(3), 1823–1846. https://doi.org/10.1093/gji/ggu369

Mayer-Gürr, T., Behzadpour, S., Ellmer, M., Kvas, A., Klinger, B., & Zehentner, N. (2016). *ITSG-Grace2016—Monthly and daily gravity field solutions from GRACE*. Potsdam: GFZ. https://doi.org/10.5880/icgem.2016.007

Peltier, R. W., Argus, D. F., & Drummond, R. (2018). Comment on "An assessment of the ICE-6G_C (VM5a) glacial isostatic adjustment model" by Purcell et al. *Journal of Geophysical Research: Solid Earth*, *123*, 2019–2028. https://doi.org/10.1002/2016JB013844

Rietbroek, R., Brunnabend, S. E., Kusche, J., Schröter, J., & Dahle, C. (2016). Revisiting the contemporary sea-level budget on global and regional scales. *Proceedings of the National Academy of Sciences*, *113*(6), 1504–1509. https://doi.org/10.1073/pnas.1519132113

Sasgen, I., Klemann, V., & Martinec, Z. (2012). Towards the inversion of GRACE gravity fields for present-day ice-mass changes and glacial-isostatic adjustment in North America and Greenland. *Journal of Geodynamics*, *59-60*, 49–63. https://doi.org/10.1016/j.jog.2012.03.004

Sasgen, I., Martín-Español, A., Horvath, A., Klemann, V., Petrie, E. J., Wouters, B., & Drinkwater, M. R. (2017). Joint inversion estimate of regional glacial isostatic adjustment in Antarctica considering a lateral varying Earth structure (ESA STSE Project REGINA). *Geophysical Journal International*, *211*(3), 1534–1553. https://doi.org/10.1093/gji/ggx368

Steffen, H., Li, T., Wu, P., Gowan, E., Ivins, E. R., Lecavalier, B., & Whitehouse, P. L. (2017). *GIA (correction) for hydrology*. Oberpfaffenhofen: Deutsches Zentrum für Luft- und Raumfahrt.

Sun, Y., Riva, R., & Ditmar, P. (2016). Optimizing estimates of annual variations and trends in geocenter motion and J 2 from a combination of GRACE data and geophysical models. *Journal of Geophysical Research: Solid Earth*, *121*, 8352–8370. https://doi.org/10.1002/2016JB013073

Swenson, S., & Wahr, J. (2002). Methods for inferring regional surface-mass anomalies from Gravity Recovery and Climate Experiment (GRACE) measurements of time-variable gravity. *Journal of Geophysical Research*, *107*(B9), ETG 3–1–ETG 3–13. https://doi.org/10.1029/2001JB000576

Tamisiea, M. E., Hill, E. M., Ponte, R. M., Davis, J. L., Velicogna, I., & Vinogradova, N. T. (2010). Impact of self-attraction and loading on the annual cycle in sea level. *Journal of Geophysical Research*, *115*, C07004. https://doi.org/10.1029/2009JC005687

Tapley, B. D., Bettadpur, S., Ries, J. C., Thompson, P. F., & Watkins, M. M. (2004). GRACE measurements of mass variability in the Earth system. *Science*, *305*(5683), 503–505. https://doi.org/10.1126/science.1099192

Tapley, B. D., Watkins, M. M., Flechtner, F., Reigber, C., Bettadpur, S., Rodell, M., & Velicogna, I. (2019). Contributions of GRACE to understanding climate change. *Nature Climate Change*, *9*, 358–369. https://doi.org/10.1038/s41558-019-0456-2

Uebbing, B., Kusche, J., Rietbroek, R., & Landerer, F. W. (2019). Processing choices affect ocean mass estimates from GRACE. *Journal of Geophysical Research: Oceans*, *124*, 1029–1044. https://doi.org/10.1029/2018JC014341

van der Wal, W., Whitehouse, P. L., & Schrama, E. J. (2015). Effect of GIA models with 3D composite mantle viscosity on GRACE mass balance estimates for Antarctica. *Earth and Planetary Science Letters*, *414*, 134–143. https://doi.org/10.1016/j.epsl.2015.01.001

Vishwakarma, B. D., Horwath, M., Devaraju, B., Groh, A., & Sneeuw, N. (2017). A data-driven approach for repairing the hydrological catchment signal damage due to filtering of GRACE products. *Water Resources Research*, *53*, 9824–9844. https://doi.org/10.1002/2017WR021150

Wahr, J. M. (2009). Time variable gravity from satellites, *Treatise on geophysics: Geodesy* (pp. 213–237). Amsterdam: Elsevier.

Wahr, J. M., Molenaar, M., & Bryan, F. (1998). Time variability of the Earth's gravity field: Hydrological and oceanic effects and their possible detection using GRACE. *Journal of Geophysical Research*, *103*, 30,205–30,229. https://doi.org/10.1029/98JB02844

Whitehouse, P. L. (2018). Glacial isostatic adjustment modelling: Historical perspectives, recent advances, and future directions. *Earth Surface Dynamics*, *6*(2), 401–429. https://doi.org/10.5194/esurf-6-401-2018

Wu, X., Heflin, M. B., Ivins, E. R., & Fukumori, I. (2006). Seasonal and interannual global surface mass variations from multisatellite geodetic data. *Journal of Geophysical Research*, *111*, B09401. https://doi.org/10.1029/2005JB004100

Yuan, D. N. (2018). JPL level-2 processing Standards document (for level-2 product release 06). GRACE Publication 327-744. ftp://isdcftp.gfz-potsdam.de/grace/DOCUMENTS/%0DLevel-2/